Electrical Power and Energy Systems 153 (2023) 109287

Contents lists available at ScienceDirect

International Journal of Electrical Power and Energy Systems

journal homepage: www.elsevier.com/locate/ijepes

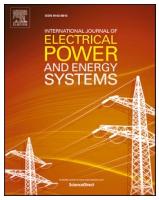

Low carbon economic dispatch of integrated energy systems considering life cycle assessment and risk cost

Min Wu [a], Jiazhu Xu [a,b,*], Yun Li [a], Linjun Zeng [c], Zhenglu Shi [a], Yuxing Liu [a], Ming Wen [b], Chang Li [d]

[a] College of Electrical and Information Engineering, Hunan University, Changsha, China
[b] Hunan Key Laboratory of Energy Internet Supply-demand and Operation, Changsha, China
[c] School of Energy and Power Engineering, Changsha University of Science and Technology, Changsha, China
[d] School of Electrical and Electronic Engineering, Nanyang Technological University, Singapore, Singapore

ARTICLE INFO

Keywords:
Conditional value-at-risk
Integrated energy system
Ladder-type carbon trading
Life cycle assessment
Low carbon economy dispatch

ABSTRACT

Integrated energy systems (IES) strengthen the interaction among electricity, gas and heat systems, and the concept of low-carbon development can further reduce the carbon emissions of IES. However, the uncertainty of IES reduces the supply flexibility and the complexity of different energy chains reduces the accuracy of carbon trading volume. Therefore, this study proposes a low carbon economic scheduling of IES considering life cycle assessment (LCA) and risk cost. First, the carbon emissions generated from different energy chain conversion processes in IES are analyzed by life cycle assessment method. Subsequently, the calculated carbon emission coefficients are introduced into the ladder-type carbon trading mechanism to further constrain the carbon emissions of IES. Specifically, the system risk is controlled using the conditional value-at-risk (CVaR) theory to obtain the day-ahead dispatch strategy. Finally, the effectiveness of the proposed method is verified based on the modified IEEE 39-node electric network, 20-node gas network and 6-node heat network models.

1. Introduction

Integrated energy system (IES) couples multiple energy sources for combined supply [1,2], which can meet the terminal load demand, realize complementary advantages among different energy sources and has been widely used [3,4]. However, most of the current studies focus on the economics of IES, ignoring the huge potential of IES to achieve carbon emission reduction[5,6]. Therefore, in order to achieve a low-carbon transition, it is necessary for IES to accelerate the promotion of low-carbon policies and related technologies.

The consumption of clean energy is an important way to save energy and reduce emissions, but the anti-peaking characteristic of wind power leads to a particularly prominent problem of wind curtailment. Power-to-gas (PtG) technology can convert surplus electricity into natural gas [7], which greatly improves the consumption of wind power. To enhance the economic and environmental benefits, an IES containing PtG constructs a new low-carbon operational framework by introducing a carbon-constrained locational marginal price[8].The hybrid energy storage of hydrogen and batteries generated by PtG can form an off-grid wind-hydrogen coupling system, confirming the ability of PtG to consume [9]. Carbon capture and storage (CCS) is a decarbonization technology for thermal power plants, which combined with PtG can significantly reduce carbon emissions. On the one hand, PtG can promote clean energy consumption [10,11]; on the other hand, CCS has significant carbon reduction capacity, which can be used to participate in the carbon trading market [12,13]. However, the above studies only focuses on the clean energy consumption capacity and carbon capture benefits [14], ignoring the incentives for PtG and CCS to participate in the carbon trading market.

The implementation of carbon emissions trading (CET) mechanism has effectively promoted carbon emission reduction from a policy perspective. IES scheduling model can reduce carbon emissions by introducing CET and carbon emission cost [15]. A low-carbon economic dispatch model for an electricity-gas system is proposed [16], which considers CCS, CET, demand response, and renewable energy, and investigates the impact of different low-carbon technologies on system economics and carbon emissions. However, the above CET calculates carbon emissions only from the perspective of energy use, but fails to

* Corresponding author at: College of Electrical and Information Engineering, Hunan University, Changsha, China.
E-mail address: xjz@hnu.edu.cn (J. Xu).

https://doi.org/10.1016/j.ijepes.2023.109287
Received 29 November 2022; Received in revised form 5 May 2023; Accepted 2 June 2023
Available online 14 June 2023

consider the total emissions of energy in the production, transmission chain in an integrated manner, as will be tackled herein.

Life cycle assessment (LCA) method is a widely used evaluation method in the electric energy chain to record the carbon emission trajectory at all stages from energy production, transportation to use [17]. The LCA method allows a comprehensive analysis of carbon emissions over the life cycle of a wind power project, providing guidance for the construction of wind farm projects [18]. However, there is little literature considering carbon trajectories in IES in a comprehensive manner. Therefore, this paper will classify all energy chains contained within the system, and apply the LCA to fully consider the carbon trajectory of each energy chain from the production source to the load demand side.

Meanwhile, large-scale grid-connected renewable energy generation has effectively alleviated energy shortage, but its uncertainty poses a great challenge to the optimal scheduling. To deal with the uncertainty, methods such as interval optimization [19,20], stochastic optimization [21–23] and robust optimization [24,25] are commonly used. All the above methods have certain shortcomings: 1) the principle of interval optimization is simple, and the interval solution can determine the upper and lower bounds, limiting the optimal solution to an interval range, which does not meet the demand for optimal solution in practical engineering. 2) Stochastic optimization uses scenario generation to obtain the expected solution of the uncertain model, which can fully consider the uncertainty in the system, but requires the probability distribution of the random parameters. 3) Robust optimization find the optimal solution under the worst scenario, strictly satisfying all constraints under the uncertainty set, but requires sacrificing some conservatism taking into account the economic efficiency. In addition, these methods do not explore in depth the potential risk of increased uncertainty and cannot analyze the severity of the scheduling risk caused by uncertainty.

In market transactions, conditional value-at-risk (CVaR) is an effective method to measure return risk and can be used to deal with uncertainty in a system. The use of CVaR as a risk constraint can constrain the risk faced by the system, which in turn improves the system operating economy and reliability [26]. CVaR can assess the risk posed by system uncertainty and form a cost-CVaR model for determining the optimal market standby demand [27]. Based on this, Ref [28] used CVaR to measure the risk loss due to wind power uncertainty and discussed the generation optimization scheduling process analytically. Risk management address the problem of wind power uncertainty leading to inability to predict accurately [29]. However, although the above literature considers the uncertainty risk, it is not translated into risk cost to be included in the economic model of system operation. In contrast, the uncertainty risk will have impact on the operation of the system, so the risk cost should be included in the economic model.

In summary, the existing scheduling schemes neither consider carbon emissions of all parts of IES comprehensively, nor ignore the uncertainty risk cost in IES. To fill in the gaps and tackle the existing issues, this study proposes an IES low-carbon economy scheduling method that considers LCA carbon emissions and risk costs. The main contributions of this study are summarized as follows.

(1) The established low-carbon economic dispatch model couples the electricity-gas-heat network and considers the coupling relationship between PtG and CCS, which can effectively realize the recycling of carbon.
(2) For the source-load uncertainty and the resulting risk in IES, we use stochastic optimization to handle the uncertainty in IES and quantify the cost of risk by CVaR, which effectively reduces the blindness of uncertainty decisions.
(3) We used the LCA method to comprehensively analyze the carbon emissions generated by different energy chains in the conversion process, and introduced carbon emission factors into the ladder-type CET mechanism to enhance enterprises' willingness to reduce emissions.

The remainders of this paper are structured as follows. The IES framework is presented in Section 2. Section 3 introduces the reward-and-punishment ladder CET based on the LCA energy chain. Section 4 develops the low-carbon economic dispatch model. Section V presents case studies under various operating conditions. Section VI concludes the paper.

2. System structure of the IES

Fig. 1 shows the overall framework of the IES. The IES in this paper consists of three parts: source side includes thermal power (TP), wind turbine (WT) and gas source (GS); network side includes gas turbine (GT), combined heat and power (CHP) unit, gas boiler (GB), battery unit (BU), CCS and PtG; load side includes electric, heat and gas load. In the power network, TP, GT, WT and CHP jointly supply power to the electric load, TP is retrofitted with CCS to capture and sequester CO2, PtG consumes part of the abandoned wind and converts CO2 to natural gas. In the gas network, the gas source and PtG supply gas to GT, CHP, GB and gas load, where CHP and GB are working together to meet the heat load demand of customers.

2.1. Energy hub model

2.1.1. Coupling device constraints

GT:

$$P_e^{\mathrm{GT}}(t) = \varepsilon_{\mathrm{gas}}^{\mathrm{LHV}} \eta^{\mathrm{GT}} V_g^{\mathrm{GT}}(t) \tag{1}$$

$$\underline{V}_g^{\mathrm{GT}} \leqslant V_g^{\mathrm{GT}}(t) \leqslant \overline{V}_g^{\mathrm{GT}} \tag{2}$$

where P_e^{GT} and V_g^{GT} are the output power and the input gas of GT respectively; η^{GT} denote the electric efficiency of GT; $\overline{V}_g^{\mathrm{GT}}$ and $\underline{V}_g^{\mathrm{GT}}$ denote the upper and lower limits of input gas of GT respectively; $\varepsilon_{\mathrm{gas}}^{\mathrm{LHV}}$ is the calorific value of gas.

GB:

$$Q_h^{\mathrm{GB}}(t) = \eta^{\mathrm{GB}} V_g^{\mathrm{GB}}(t) \tag{3}$$

$$\underline{V}_g^{\mathrm{GB}} \leqslant V_g^{\mathrm{GB}}(t) \leqslant \overline{V}_g^{\mathrm{GB}} \tag{4}$$

where Q_h^{GB} and V_g^{GB} denote the output heat power and the input gas of GB respectively; η^{GB} denote the heat efficiency of GB; $\overline{V}_g^{\mathrm{GB}}$ and $\underline{V}_g^{\mathrm{GB}}$ denote the upper and lower limits of input natural gas of GB respectively.

CHP:

Fig. 2 shows the thermoelectric output of CHP. The CHP is capable of

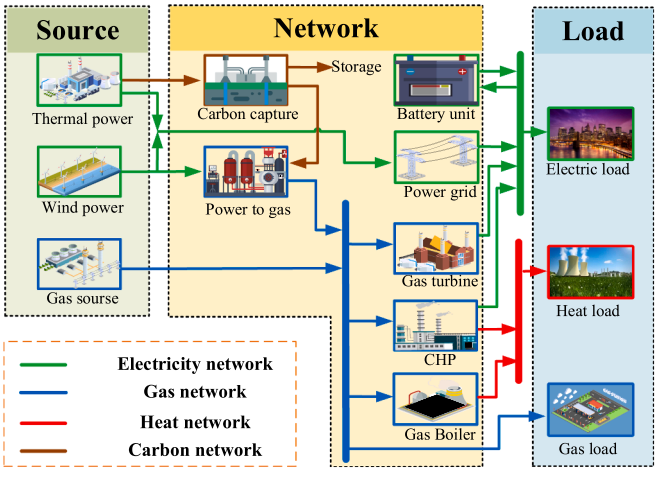

Fig. 1. The overall framework of IES.

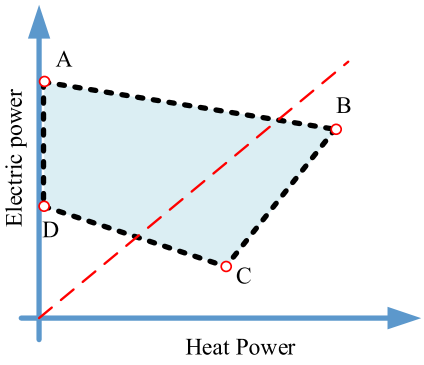

Fig. 2. The thermoelectric output of CHP.

producing both electricity and heat, and there is an "electro-thermal characteristic" of the power and heat generated. The polygon area ABCD in Fig. 2 illustrates the combined heat and power feasible domain for the CHP unit. The efficiency of the CHP unit is a constant, as shown by the red dashed line in the Fig. 2.

The electric power and thermal power emitted by CHP can be represented by the extreme points in the polygon region.

$$P_e^{\mathrm{CHP}}(t)=\sum_{z=1}^{N_z}\alpha^z(t)P_e^z \tag{5}$$

$$Q_h^{\mathrm{CHP}}(t)=\sum_{z=1}^{N_z}\alpha^z(t)Q_h^z \tag{6}$$

$$\sum_{z=1}^{N_z}\alpha^z(t)=1,0\leqslant\alpha^z(t)\leqslant1 \tag{7}$$

where P_e^{CHP} and Q_h^{CHP} are the electric power and heat power of CHP; P_e^{CHP} and Q_h^{CHP} denote the electric power and thermal power at the z-th extreme point; N_z denotes the number of extreme points; α^z is the operating point of the CHP.

2.1.2. Power network constraints

The active power at node j of the distribution system at time t can be expressed as:

$$\begin{aligned}P_{j,t}=&\sum_{l\in\Omega_j^{\mathrm{BU}}}\left(P_{e,\mathrm{out}}^{\mathrm{BU}}(l,t)-P_{e,\mathrm{in}}^{\mathrm{BU}}(l,t)\right)+\sum_{l\in\Omega_j^{\mathrm{TP}}}P_{l,t}^{\mathrm{TP}}+\sum_{l\in\Omega_j^{\mathrm{GT}}}P_{l,t}^{\mathrm{GT}}\\&+\sum_{l\in\Omega_j^{\mathrm{CHP}}}P_{l,t}^{\mathrm{CHP}}+\sum_{l\in\Omega_j^{\mathrm{WT}}}\left(P_{l,t}^{\mathrm{WT}}-P_{l,t}^{\mathrm{WT,shed}}\right),\forall j\in\mathscr{N}_e,\forall t\in\mathscr{T}\end{aligned} \tag{8}$$

where $\mathscr{N}_e$ is the set of all nodes of the power network; $\mathscr{T}$ is the dispatch period; l is the l-th device in the corresponding set.$P_{l,t}^{\mathrm{TP}}$,$P_{l,t}^{\mathrm{GT}}$, $P_{l,t}^{\mathrm{WT}}$ and $P_{l,t}^{\mathrm{CHP}}$ denote the active output power of TP, GT, WT, CHP at moment t; $P_{\mathrm{e,in}}^{\mathrm{BU}}$ and $P_{\mathrm{e,out}}^{\mathrm{BU}}$ denote the charge and discharge power of BU;$P_{l,t}^{\mathrm{WT,shed}}$ and $P_{l,t}^{\mathrm{WT}}$ denote the wind curtailment and forecast power at moment t;Ω_j^{TP},Ω_j^{GT}, Ω_j^{BU} and Ω_j^{WT} are the sets of corresponding device at node j, respectively.

The power flow constraint adopts the DC power flow constraint, the unit climbing constraint and the minimum on/off constraint are detailed in the [30].

2.1.3. Natural gas network constraints

The injected gas in node j of the gas network at moment t satisfies the gas flow balance constraint:

$$\begin{aligned}\sum_{j\in\mathscr{N}_g,j\neq i}V_{j,t}+\sum_{l\in\Omega_j^{\mathrm{PtG}}}V_{l,t}^{\mathrm{PtG}}=&\sum_{l\in\Omega_j^{\mathrm{GT}}}V_{l,t}^{\mathrm{GT}}+\sum_{l\in\Omega_j^{\mathrm{CHP}}}V_{l,t}^{\mathrm{CHP}}+\sum_{l\in\Omega_j^{\mathrm{GB}}}V_{l,t}^{\mathrm{GB}}\\&+L_{g,j,t},\forall(i,j)\in\mathscr{N}_g,\forall ij\in\mathscr{L}_g,\forall t\in\mathscr{T}\end{aligned} \tag{9}$$

where $\mathscr{N}_g$ is the set of all nodes of the gas network; $\mathscr{L}_g$ is the set of all pipes of the gas network; $V_{j,t}$ is the gas volume of node j at time t; $V_{l,t}^{\mathrm{PtG}}$ denotes the volume of gas injected by PtG at time t;$V_{l,t}^{\mathrm{GT}}$,$V_{l,t}^{\mathrm{CHP}}$, $V_{l,t}^{\mathrm{GB}}$ and $L_{g,j,t}$ represent the volume of gas consumed by GT, CHP, GB and load at time t, respectively;Ω_j^{PtG},Ω_j^{GT}, Ω_j^{CHP} and Ω_j^{GB} are the sets of each device at node j, respectively.

In this paper, we consider the bidirectional flow of natural gas in pipelines, where the flow rate is related to the air pressure at both ends of the pipeline and its own properties.

$$V_{ij,t}=K_{ij}S_{ij,t}\sqrt{S_{ij,t}\left(p_{i,t}^2-p_{j,t}^2\right)},\forall(i,j)\in\mathscr{N}_g,\forall ij\in\mathscr{L}_g \tag{10}$$

$$S_{ij,t}=\begin{cases}1, & p_{i,t}\geqslant p_{j,t}\\ -1, & p_{i,t}<p_{j,t}\end{cases},\forall(i,j)\in\mathscr{N}_g,\forall ij\in\mathscr{L}_g \tag{11}$$

$$\left|V_{ij,t}\right|\leqslant\overline{V}_{ij},\forall ij\in\mathscr{L}_g \tag{12}$$

$$\underline{p}_i\leqslant p_{i,t}\leqslant\overline{p}_i,\forall i\in\mathscr{N}_g \tag{13}$$

where $V_{ij,t}$ is the gas volume of pipeline ij at time t; K_{ij} is the transmission coefficient; $S_{ij,t}$ denotes the direction of gas flow, and a value of 1 indicates flow from the initial node to the end node, and the opposite for -1; $p_{i,t}$ and $p_{j,t}$ are the air pressure at the corresponding node at time t; $\overline{V}_{ij}$ is the upper limit in pipeline ij; $\underline{p}_i$ and $\overline{p}_i$ are the upper and lower limits of air pressure at node i, respectively.

2.1.4. Heat network constraints

Fig. 3 shows the node schematic of the heating network. In Fig. 3, S_i^+ and S_i^- denote the set of pipes starting and ending at the i-th node;$T_{p,t}^{\mathrm{S,in}}$ and $T_{p,t}^{\mathrm{S,out}}$ denote the inlet and outlet water temperature of pipe p in the water supply network; $T_{p,t}^{\mathrm{R,in}}$ and $T_{p,t}^{\mathrm{R,out}}$ denote the inlet and outlet water temperature of pipe p in the return water network; $T_{i,t}^{\mathrm{S}}$ and $T_{i,t}^{\mathrm{R}}$ denote the mixing temperatures of the water supply and return systems at node i; $m_{p,t}^{\mathrm{S}}$ and $m_{p,t}^{\mathrm{R}}$ denote the hot water flow rate of the p-th pipe in the water supply and return network at time t.

The water flow in a heat pipe is assumed to be single dimensional and incompressible. Therefore, the hot water distribution obeys the continuity equation, the inflow hot water at any node is equal to the outflow hot water.

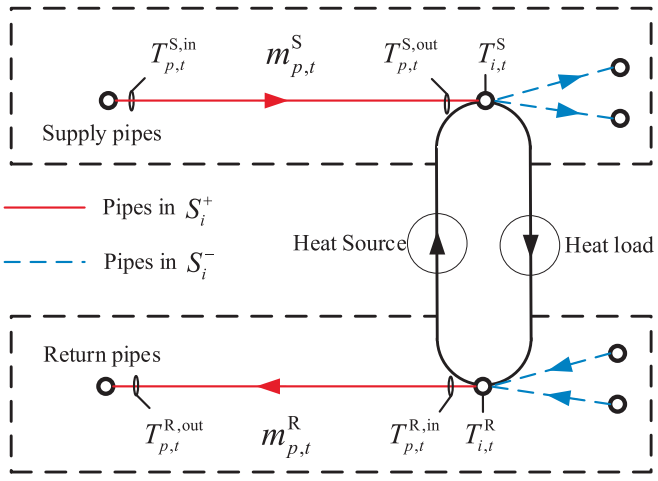

Fig. 3. Node schematic of the heating network.

$$\sum_{p\in S_i^+} m_{p,t}^{\mathrm{S}} = \sum_{p\in S_i^-} m_{p,t}^{\mathrm{R}}, \forall i \in \mathscr{N}_h, \forall t \in \mathscr{T} \tag{14}$$

where $\mathscr{N}_h$ denotes the set of heat system nodes.

Based on the principle of energy conservation, the nodal temperature mixing process can be expressed as:

$$\sum_{p\in S_i^-} \left(T_{p,t}^{\mathrm{S,out}} m_{p,t}^{\mathrm{S}}\right) = T_{i,t}^{\mathrm{S}} \sum_{p\in S_i^-} m_{p,t}^{\mathrm{S}}, \forall i \in \mathscr{N}_h, \forall t \in \mathscr{T} \tag{15}$$

$$\sum_{p\in S_i^+} \left(T_{p,t}^{\mathrm{R,out}} m_{p,t}^{\mathrm{R}}\right) = T_{i,t}^{\mathrm{R}} \sum_{p\in S_i^+} m_{p,t}^{\mathrm{R}}, \forall i \in \mathscr{N}_h, \forall t \in \mathscr{T} \tag{16}$$

$$T_{p,t}^{\mathrm{S,out}} = T_{i,t}^{\mathrm{S}}, T_{p,t}^{\mathrm{R,in}} = T_{i,t}^{\mathrm{R}}, \forall (i,j) \in \mathscr{L}_h, \forall t \in \mathscr{T} \tag{17}$$

where Eq. (15) and Eq. (16) are the nodal temperature balance constraints, and Eq. (17) indicates the correlation between the inlet water temperature of the pipes and the nodal water temperature.

The heat exchange process between the heat source and the heat load can be expressed as:

$$\sum_{l\in\Omega_j^{\mathrm{CHP}}} Q_{l,t}^{\mathrm{CHP}} + \sum_{l\in\Omega_j^{\mathrm{GB}}} Q_{l,t}^{\mathrm{GB}} = c_w m_{i,t}^{\mathrm{in}} \left(T_{i,t}^{\mathrm{S}} - T_{i,t}^{\mathrm{R}}\right) \quad \forall j \in \mathscr{N}_h, \forall t \in \mathscr{T} \tag{18}$$

$$\sum_{l\in\Omega_j^{\mathrm{CHP}}} Q_{l,t}^{\mathrm{CHP}} + \sum_{l\in\Omega_j^{\mathrm{GB}}} Q_{l,t}^{\mathrm{GB}} = L_{h,i,t} \tag{19}$$

where $Q_{l,t}^{\mathrm{CHP}}$ and $Q_{l,t}^{\mathrm{GB}}$ denote the output heat of CHP and GB at time t; $m_{i,t}^{\mathrm{in}}$ denote the hot water flow rate of the heat source at node j; $L_{h,i,t}$ is the heat load of heat system at time t; c_w is the specific heat capacity of water.

2.1.5. Energy storage constraints

$$S_e^{\mathrm{BU}}(t+1) = S_e^{\mathrm{BU}}(t) + \frac{\eta_{\mathrm{in}}^{\mathrm{BU}} P_{e,\mathrm{in}}^{\mathrm{BU}}(t) - P_{e,\mathrm{out}}^{\mathrm{BU}}(t) \Big/ \eta_{\mathrm{out}}^{\mathrm{BU}}}{C_e^{\mathrm{BU}}} \tag{20}$$

$$\underline{S}_e^{\mathrm{BU}} \leqslant S_e^{\mathrm{BU}}(t) \leqslant \overline{S}_e^{\mathrm{BU}} \tag{21}$$

$$S_e^{\mathrm{BU}}(t)|_{t=1} = S_e^{\mathrm{BU}}(t)|_{t=T+1} \tag{22}$$

$$v_{\mathrm{in}}^{\mathrm{BU}}(t)\underline{P}_{e,\mathrm{in}}^{\mathrm{BU}} \leqslant P_{e,\mathrm{in}}^{\mathrm{BU}}(t) \leqslant v_{\mathrm{in}}^{\mathrm{BU}}(t)\overline{P}_{e,\mathrm{in}}^{\mathrm{BU}} \tag{23}$$

$$v_{\mathrm{out}}^{\mathrm{BU}}(t)\underline{P}_{e,\mathrm{out}}^{\mathrm{BU}} \leqslant P_{e,\mathrm{out}}^{\mathrm{BU}}(t) \leqslant v_{\mathrm{out}}^{\mathrm{BU}}(t)\overline{P}_{e,\mathrm{out}}^{\mathrm{BU}} \tag{24}$$

$$v_{\mathrm{in}}^{\mathrm{BU}}(t) + v_{\mathrm{out}}^{\mathrm{BU}}(t) = 1 \tag{25}$$

where S_e^{BU} is the charge level of BU, $\overline{S}_e^{\mathrm{BU}}$ and $\underline{S}_e^{\mathrm{BU}}$ are the upper and lower limits; $v_{\mathrm{in}}^{\mathrm{BU}}$ and $v_{\mathrm{out}}^{\mathrm{BU}}$ are the charge and discharge state; C_e^{BU} is the battery capacity; $\eta_{\mathrm{in}}^{\mathrm{BU}}$ and $\eta_{\mathrm{out}}^{\mathrm{BU}}$ represent the charge efficiency and discharge efficiency of BU.

Eq. (20) indicates the dynamic constraint; Eq. (21) is the upper and lower limit constraint; Eq. (22) is the time-domain decoupling constraint of BU; Eq. (23) and Eq. (24) are the upper limit constraint of BU charging and discharging; Eq. (25) means that BU cannot charge and discharge at the same time.

2.2. PtG-CCS model

CCS can capture the CO_2 released during TP power generation and reduce the carbon emission. PtG can consume abandoned wind and convert CO_2 to natural gas. The coupling of PtG and CCS can enhance the economic efficiency, which is an important means to achieve IES decarbonization.

Fig. 4 shows the coupling relationship of PtG-CCS. PtG can convert CO_2 into natural gas to improve the consumption rate of clean energy, while CCS can collect and store CO_2 to reduce the carbon emission of the system. The coupling of PtG and CCS can effectively realize the recycling of CO_2, which has good economic and environmental benefits.

2.2.1. CCS

The carbon emission of TP is much higher than GT with the same electrical power output. Therefore, CCS is generally modified accordingly for TP to significantly reduce the carbon emissions of the unit. CCS has a base energy consumption $P_{e,\mathrm{base}}^{\mathrm{CCS}}$ and an operational energy consumption$P_{e,\mathrm{run}}^{\mathrm{CCS}}$, where the base energy consumption is related to the rated capacity and the operational energy consumption is proportional to the CO_2 captured.

$$P_e^{\mathrm{CCS}}(t) = P_{e,\mathrm{base}}^{\mathrm{CCS}}(t) + P_{e,\mathrm{run}}^{\mathrm{CCS}}(t) \tag{26}$$

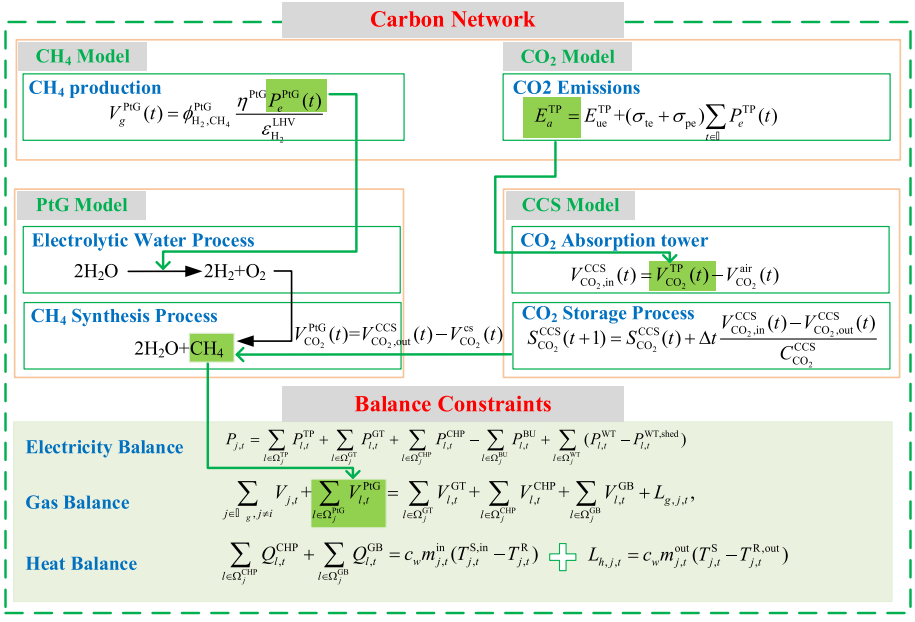

Fig. 4. PtG-CCS coupling framework.

$$P^{\mathrm{CCS}}_{e,\mathrm{base}}(t) = \varepsilon^{\mathrm{CCS}}_{e}\eta^{\mathrm{CCS}}C^{\mathrm{CCS}}_{\mathrm{CO_2}} \tag{27}$$

$$P^{\mathrm{CCS}}_{e,\mathrm{run}}(t) = \eta^{\mathrm{CCS}}V^{\mathrm{CCS}}_{\mathrm{CO_2,in}}(t) \tag{28}$$

where η^{CCS} denotes the power consumption per unit of CO_2 captured; $\varepsilon^{\mathrm{CCS}}_{e}$ is a ratio of the base energy consumption; $C^{\mathrm{CCS}}_{\mathrm{CO_2}}$ represents the capacity of CCS; $V^{\mathrm{CCS}}_{\mathrm{CO_2,in}}$ is the volume of captured CO_2.

A portion of the carbon emissions from TP is absorbed by CCS and the rest is emitted to the atmosphere. The input carbon of CCS is:

$$V^{\mathrm{CCS}}_{\mathrm{CO_2,in}}(t) = V^{\mathrm{TP}}_{\mathrm{CO_2}}(t) - V^{\mathrm{air}}_{\mathrm{CO_2}}(t) \tag{29}$$

$$V^{\mathrm{TP}}_{\mathrm{CO_2}}(t) = \eta^{\mathrm{TP}}_{\mathrm{CO_2}}P^{\mathrm{TP}}_{e}(t) \tag{30}$$

where $V^{\mathrm{air}}_{\mathrm{CO_2}}$ is the volume of CO_2 emitted to air; $V^{\mathrm{TP}}_{\mathrm{CO_2}}$ is the volume of CO_2 output of TP; $\eta^{\mathrm{TP}}_{\mathrm{CO_2}}$ is the CO_2 emitted per unit of electrical power generated by TP.

In this paper, the CO_2 absorbed by CCS was used as unique carbon source for PtG, and the rest was sequestered to the subsurface by transportation. The output carbon of CCS is:

$$V^{\mathrm{CCS}}_{\mathrm{CO_2,out}}(t) = V^{\mathrm{PtG}}_{\mathrm{CO_2}}(t) + V^{\mathrm{cs}}_{\mathrm{CO_2}}(t) \tag{31}$$

where $V^{\mathrm{PtG}}_{\mathrm{CO_2}}$ is the volume of CO_2 absorbed by PtG; $V^{\mathrm{cs}}_{\mathrm{CO_2}}$ is the volume of CO_2 sequestered into the ground.

The CCS includes a carbon storage unit with similar input and output constraints as the energy storage unit.

$$S^{\mathrm{CCS}}_{\mathrm{CO_2}}(t+1) = S^{\mathrm{CCS}}_{\mathrm{CO_2}}(t) + \frac{V^{\mathrm{CCS}}_{\mathrm{CO_2,in}}(t) - V^{\mathrm{CCS}}_{\mathrm{CO_2,out}}(t)}{C^{\mathrm{CCS}}_{\mathrm{CO_2}}} \tag{32}$$

$$\underline{S}^{\mathrm{CCS}}_{\mathrm{CO_2}} \leqslant S^{\mathrm{CCS}}_{\mathrm{CO_2}}(t) \leqslant \overline{S}^{\mathrm{CCS}}_{\mathrm{CO_2}} \tag{33}$$

$$S^{\mathrm{CCS}}_{\mathrm{CO_2}}(t)|_{t=1} = S^{\mathrm{CCS}}_{\mathrm{CO_2}}(t)\Big|_{t=T+1} \tag{34}$$

$$0 \leqslant V^{\mathrm{CCS}}_{\mathrm{CO_2,in}}(t) \leqslant \overline{V}^{\mathrm{CCS}}_{\mathrm{CO_2}} \tag{35}$$

$$0 \leqslant V^{\mathrm{CCS}}_{\mathrm{CO_2,out}}(t) \leqslant \overline{V}^{\mathrm{CCS}}_{\mathrm{CO_2}} \tag{36}$$

where $S^{\mathrm{CCS}}_{\mathrm{CO_2}}$ is the carbon storage state of the CCS with upper bounds $\overline{S}^{\mathrm{CCS}}_{\mathrm{CO_2}}$ and lower bounds$\underline{S}^{\mathrm{CCS}}_{\mathrm{CO_2}}$; $\overline{V}^{\mathrm{CCS}}_{\mathrm{CO_2}}$ is the input and output limits of CCS.

2.2.2. PtG

The production of gas from PtG requires two stages. The first stage is carried out in the electrolysis plant, using the surplus electrical energy during the abandonment period to decompose water into H_2 and O_2. The electrical input power P^{PtG}_{e} and the H_2 output $V^{\mathrm{PtG}}_{\mathrm{H_2}}$ have the following relationship:

$$V^{\mathrm{PtG}}_{\mathrm{H_2}}(t) = \frac{\eta^{\mathrm{PtG}}P^{\mathrm{PtG}}_{e}(t)}{\varepsilon^{\mathrm{LHV}}_{\mathrm{H_2}}} \tag{37}$$

$$v^{\mathrm{PtG}}\underline{P}^{\mathrm{PtG}}_{e} \leqslant P^{\mathrm{PtG}}_{e}(t) \leqslant v^{\mathrm{PtG}}\overline{P}^{\mathrm{PtG}}_{e} \tag{38}$$

where η^{PtG} is the efficiency of electric hydrogen production; $\varepsilon^{\mathrm{LHV}}_{\mathrm{H_2}}$ are the high calorific value of H_2; $\underline{P}^{\mathrm{PtG}}_{e}$ and $\overline{P}^{\mathrm{PtG}}_{e}$ denotes the minimum and maximum input power; v^{PtG} is the operating state of the electrolysis equipment.

The second stage takes place in the methanation plant, where H_2 and CO_2 undergo the Sabatier reaction to synthesize methane and water. In the Sabatier reaction, the relationship among CO_2, H_2 and gas is:

$$V^{\mathrm{PtG}}_{\mathrm{CO_2}}(t) = V^{\mathrm{PtG}}_{\mathrm{H_2}}(t)\phi^{\mathrm{PtG}}_{\mathrm{H_2,CO_2}} \tag{39}$$

$$V^{\mathrm{PtG}}_{g}(t) = V^{\mathrm{PtG}}_{\mathrm{H_2}}(t)\phi^{\mathrm{PtG}}_{\mathrm{H_2,CH_4}} \tag{40}$$

where $\phi^{\mathrm{PtG}}_{\mathrm{H_2,CO_2}}$ denotes the reaction coefficient between H_2 and CO_2; $\phi^{\mathrm{PtG}}_{\mathrm{H_2,CH_4}}$ is the reaction coefficient between H2 and CH4.

3. Ladder CET mechanism based on LCA energy chain

The traditional carbon trading market does not have a certain ladder pricing in different difference intervals, which cannot form an effective disincentive to large-scale carbon emissions. In addition, the existing carbon trading market only considers the emissions of energy use, and fails to consider the carbon emission trajectories of production and transportation, which cannot fully account for the total emissions. Therefore, this paper adopts a LCA method to record the carbon emission trajectory at each stage from energy production, transportation to use. Meanwhile, the traditional CET mechanism is improved by adopting a step pricing format to further promote the low carbon development of the system.

3.1. Carbon emission measurement based on LCA

LCA has three steps: classification, characterization, and quantification [31]. First, the energy sources of IES are divided into coal, natural gas and wind energy, and each energy source within IES is divided into energy chains according to the order of energy activities. Subsequently, the transmission links of each energy chain are summarized and simplified. Finally, carbon emission factors are calculated based on energy activities within each link. In addition, the existing LCA-related studies consider the energy utilization link by the product of power and utilization factor for calculation, ignoring the difference in carbon emissions of different units in actual operation [32]. This study takes this difference into account and uses quadratic polynomial fitting for different types of equipment utilization links to improve the solution accuracy. Fig. 5 shows the carbon emission energy chain based on LCA.

3.1.1. Coal power

The greenhouse gas emissions of the coal power energy chain mainly come from 3 segments: coal production (mining and washing), electric coal transportation, and combustion.:

$$\begin{cases} \sigma_{\mathrm{pe}} = I_{\mathrm{cp}}\eta_{\mathrm{cp}}\chi_{\mathrm{cp}}\left(1+\delta_{\mathrm{pe},1}+\delta_{\mathrm{pe},2}\right) \\ \sigma_{\mathrm{te}} = \sum_{a\in\Omega^{\mathrm{tw}}}\sum_{b\in\Omega^{\mathrm{ft}}} I_{a,b}Q_{a,b,k}k_{a,b}M_aD_a \\ E^{\mathrm{TP}}_{\mathrm{ue}}(t) = \sum_{t\in\mathscr{T}}\left[a_1 + b_1P^{\mathrm{TP}}_{e}(t) + c_1\left(P^{\mathrm{TP}}_{e}(t)\right)^2\right] \end{cases} \tag{41}$$

where σ_{pe} is total emission coefficient of coal production, g/kWh; I_{cp} is the unit energy consumption of coal production process; η_{cp} is the conversion efficiency of coal production; χ_{cp} is the emission coefficient of coal production, g/kWh; $\delta_{\mathrm{pe},1}$ is the loss rate per unit of electricity caused by nature in the coal production process; $\delta_{\mathrm{pe},2}$ indicates the loss rate of

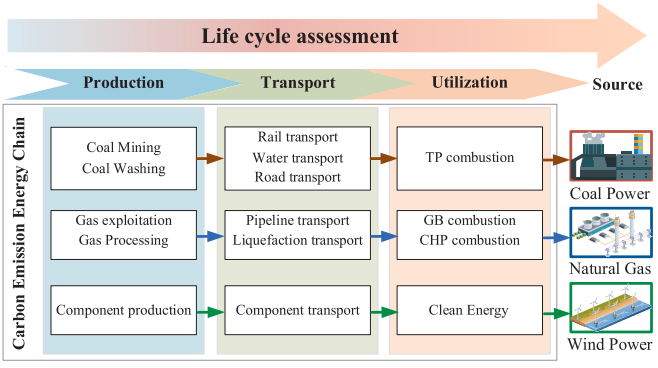

Fig. 5. Carbon emission energy chain based on LCA.

raw coal per unit of electricity occurred in the process of raw coal washing. σ_{te} is the total carbon emission coefficient of coal transportation, g/kWh; Ω^{tw} is the set of various coal transportation modes, mainly including rail, waterway and road transportation; Ω^{ft} is the set of various fuels, mainly including gasoline, diesel and electricity; $I_{a,b}$ is the energy intensity of the b-th fuel used in the a-th transport mode; $Q_{a,b,k}$ is the carbon emission factor of k-th type of greenhouse gas from the b-th fuel used in transport mode a, g/kWh; $k_{a,b}$ is the ratio of the mileage of transport mode a to the total mileage; M_a is the total amount of coal transported by type transportation mode a, t; D_a is the average transportation mileage of transportation mode a, km; E_{ue}^{TP} is the carbon emission of TP in the coal-fired power generation segment; a_1, b_1, c_1 are the quadratic term fitting coefficients of TP carbon emission.

3.1.2. Natural gas

Greenhouse gas emissions from the gas energy chain mainly include 3 links: exploitation, transportation and use.

$$\begin{cases} \sigma_{pg} = \lambda_{gl}\chi_g + \sum_{k\in\Omega^{GG}} \eta_{pg}^k \chi_{pg}^k \\ \sigma_{tg} = \delta\chi_{lt} + (1-\delta)\chi_{pt} \\ E_{ue}^{GT}(t) = \sum_{t\in\mathcal{T}} \left[a_2 + b_2 P_e^{GT}(t) + c_2\left(P_e^{GT}(t)\right)^2\right] \\ E_{ue}^{CHP}(t) = \sum_{t\in\mathcal{T}} \begin{bmatrix} a_3 + b_3\left(P_e^{CHP}(t) + Q_h^{CHP}(t)\right) \\ +c_3\left(P_e^{CHP}(t) + Q_h^{CHP}(t)\right)^2 \end{bmatrix} \end{cases} \tag{42}$$

where σ_{pg} is the total carbon emission factor of the gas production stage, g/kWh; η_{pg}^k is the conversion factor of the k-th greenhouse gas to carbon; χ_{pg}^k is the emission intensity of the k-th greenhouse gas, g/kWh; λ_{gl} is the self-fugitive rate of the natural gas extraction process; χ_g is the carbon emission intensity of gas, g/kWh; χ_{pt} and χ_{lt} are the carbon emission coefficient of pipeline transportation and liquefaction transportation respectively, g/kWh; δ is the share of pipeline transportation in the total transportation volume; E_{ue}^{GT} and E_{ue}^{CHP} represent the carbon emission of GT and CHP in coal-fired power generation; a_2, b_2, c_2 are the quadratic fitting coefficients of GT carbon emission; a_3, b_3, c_3 are the quadratic fitting coefficients of CHP carbon emission.

3.1.3. Wind power

The emission of clean energy can be divided into two stages: production and construction, and transportation. Numerous studies have shown that the carbon emissions from the operation of clean energy units are minimal and negligible.

$$\begin{cases} \sigma_{pw} = \sum_{i\in\Omega^{cm}} \eta_{en}\left[\frac{(1+\delta_i)\chi_{cp,i}}{e_{cp,i}} + \frac{\chi_{ct,i}}{e_{ct,i}} + \frac{\chi_{cp,i,j}}{e_{cp,i,j}}\right] \\ \sigma_{tw} = \sum_{i\in\Omega^{CM}} \eta_{en} e_{t,i} c_{t,i} \end{cases} \tag{43}$$

where σ_{pw} is the total emission factor of the WT production, g/kWh; δ_i is the loss factor of the i-th material required for the production unit construction; η_{en} is the conversion factor of the unit standard electricity and energy consumption, MJ/kWh; Ω^{CM} is the quantity of the type of material required for the production; $\chi_{cp,i}$ is the carbon emission intensity of the i-th material used in the construction, g/t; $e_{cp,i}$ is the value of the energy intensity embedded in the i-th material used in the construction, GJ/t; $\chi_{ct,i}$ is the carbon intensity of the i-th material in the production process, g/t; $e_{ct,i}$ is the energy intensity consumed in the transportation of materials in the production process, GJ/t; $\chi_{cp,i,j}$ is the carbon intensity of the i-th material in the j-th construction process, g/t; $e_{cp,i,j}$ is the embedded energy intensity value of the material in the i-th construction process of the j-th, GJ/t; σ_{tw} is the emission factor of the transportation of unit components, g/kWh; $c_{t,i}$ is the carbon emission intensity, g/t; $e_{t,i}$ is the energy intensity consumed for the transportation of the i-th component, GJ/t.

3.2. Reward and punishment type ladder CET mechanism

IES has significant low carbon benefits, however, the existing studies establish a simple carbon emission model and do not fully consider the guiding role of the carbon trading market. Therefore, this subsection proposes the reward and punishment ladder CET mechanism as another important means to achieve decarbonization, strengthen the carbon trading market's role in guiding carbon emissions.

3.2.1. Carbon emission quota model

The carbon trading market can effectively promote the low carbon emission reduction of various industries. The regulator issues free carbon quota to IES, and when the carbon emission generated by IES is lower than this quota, the remaining quota can be taken to the carbon trading market for sale, conversely, it needs to be purchased. The main carbon emission sources of IES are TP, GT, CHP and GB.

$$\begin{cases} E_q^{IES} = E_q^{TP} + E_q^{GT} + E_q^{CHP} + E_q^{GB} \\ E_q^{TP} = \chi_e^{TP} \sum_{t\in\mathcal{T}} P_e^{TP}(t) \\ E_q^{GT} = \chi_e^{GT} \sum_{t\in\mathcal{T}} P_e^{GT}(t) \\ E_q^{CHP} = \sum_{t\in\mathcal{T}} \left(\chi_e^{CHP} P_e^{CHP}(t) + \chi_h^{CHP} Q_h^{CHP}(t)\right) \\ E_q^{GB} = \chi_h^{GB} \sum_{t\in\mathcal{T}} P_e^{GB}(t) \end{cases} \tag{44}$$

where E_q^{IES}, E_q^{TP}, E_q^{GT}, E_q^{CHP} and E_q^{GB} represent the carbon emission quota of IES, TP, GT, CHP, GB; χ_e^{TP}, χ_e^{GT}, χ_e^{CHP}, χ_h^{CHP} and χ_h^{GB} denote the corresponding quota factors.

3.2.2. Actual carbon emissions model

In practice, CCS can reduce carbon emissions by collecting CO_2. However, existing literature has neglected this part of carbon emissions, so the existing models of actual carbon emissions are refined in the model.

$$\begin{cases} E_a^{IES} = E_a^{TP} + E_a^{GT} + E_a^{CHP} + E_a^{GB} - V_{CO_2,in}^{CCS} \\ E_a^{TP} = E_{ue}^{TP} + \left(\sigma_{te} + \sigma_{pe}\right) \sum_{t\in\mathcal{T}} P_e^{TP}(t) \\ E_a^{GT} = E_{ug}^{GT} + \left(\sigma_{tg} + \sigma_{pg}\right) \sum_{t\in\mathcal{T}} V_g^{GT}(t) \\ E_a^{CHP} = E_{ug}^{CHP} + \left(\sigma_{tg} + \sigma_{pg}\right) \sum_{t\in\mathcal{T}} V_g^{CHP}(t) \\ E_a^{GB} = \left(\sigma_{tg} + \sigma_{pg} + \chi_a^{GB}\right) \sum_{t\in\mathcal{T}} V_g^{GB}(t) \end{cases} \tag{45}$$

where: E_a^{IES}, E_a^{TP}, E_a^{GT}, E_a^{CHP} and E_a^{GB} are the actual carbon emissions of IES, GT, CHP and GB, respectively; χ_a^{GB} denotes the actual carbon emission factor of GB.

3.2.3. Ladder CET mechanism

Based on the initial carbon emission quota and the actual carbon emission model, the carbon trading volume is:

$$E^{IES} = E_a^{IES} - E_q^{IES} \tag{46}$$

Similar to the stepped electricity price, this paper uses a split carbon emission interval to calculate the cost of carbon trading. When the difference between carbon emission and carbon quota exceeds a given interval, the price of carbon trading is increased. The more carbon

allowances that need to be purchased, the higher the purchase price will be in the corresponding zone.

$$C_{\mathrm{CET}}=\begin{cases}\lambda(1+\alpha)\left(E^{\mathrm{IES}}+d\right)-\lambda d, -2d\leqslant E^{\mathrm{IES}}\leqslant -d\\ \lambda E^{\mathrm{IES}}, -d\leqslant E^{\mathrm{IES}}\leqslant d\\ \lambda(1+\alpha)\left(E^{\mathrm{IES}}-d\right)+\lambda d, d\leqslant E^{\mathrm{IES}}\leqslant 2d\\ \lambda(1+2\alpha)\left(E^{\mathrm{IES}}-2d\right)+(2+\alpha)\lambda d, 2d\leqslant E^{\mathrm{IES}}\leqslant 3d\\ \lambda(1+3\alpha)\left(E^{\mathrm{IES}}-3d\right)+(3+3\alpha)\lambda d, 3d\leqslant E^{\mathrm{IES}}\leqslant 4d\\ \lambda(1+4\alpha)\left(E^{\mathrm{IES}}-4d\right)+(4+6\alpha)\lambda d, 4d\leqslant E^{\mathrm{IES}}\end{cases} \tag{47}$$

where C_{CET} is the carbon trading cost; λ is the base price; d is the length of the interval; α is the price increase.

Fig. 6 shows the reward and punishment type ladder CET mechanism.

4. CVaR-based economic dispatch model for integrated energy systems

IES has a contradictory relationship between "increasing new energy consumption" and "avoiding quota standard penalties", and is a suitable modeling object for CVaR.

4.1. CVaR-based risk measures for probabilistic scenarios

CVaR is an improved risk analysis method proposed based on VaR (Value at Risk) [33], which can overcome the shortcoming of VaR that cannot accurately measure risk losses under adverse conditions. CVaR is defined as the average value of loss when the portfolio's risk loss is higher than the VaR.

$$\mathrm{CVaR}_{\beta}(X)=\mathbb{E}_{\mathbb{p}}\left[f(X,\xi)\middle|f(X,\xi)>\mathrm{VaR}_{\beta}\right] \tag{48}$$

$f(X,\xi)$ is the loss function of portfolio X, and ξ is the continuous random variable that may affect the loss function; $\mathbb{E}_{\mathbb{p}}$ is the expectation under the condition of$f(X,\xi)>\mathrm{VaR}_{\beta}$.

Let the probability density function of the random variable be$p(\xi)$, and the distribution function of the loss function is.

$$\phi(X,\alpha)=\int_{f(X,\xi)\leqslant\alpha}p(\xi)d\xi \tag{49}$$

For a given confidence levelβ, the VaR of portfolio is:

$$\mathrm{VaR}_{\beta}=\min\{\alpha\in\mathbb{R}|\phi(X,\alpha)>\beta\} \tag{50}$$

Then the corresponding CVaR is expressed as:

$$\begin{aligned}&\mathrm{CVaR}_{\beta}(X)=E\left[f(X,\xi)\middle|f(X,\xi)>\mathrm{VaR}_{\beta}\right]\\&=\mathrm{VaR}_{\beta}+\frac{1}{1-\beta}\int_{\xi}\max\left\{f(X,\xi)-\mathrm{VaR}_{\beta},0\right\}p(\xi)d\xi\end{aligned} \tag{51}$$

By replacing the integral in Eq. (51) using the discrete points in each probability scenario, the discrete CVaR is:

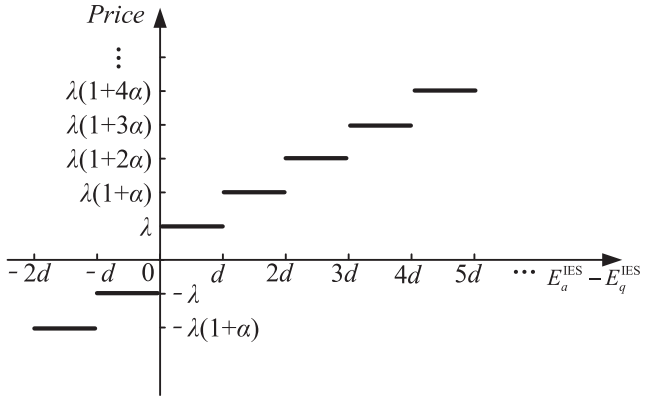

Fig. 6. Reward and punishment type ladder CET mechanism.

$$\begin{aligned}&\mathrm{CVaR}_{\beta}(X)=E\left[f(X,\xi)\middle|f(X,\xi)>\mathrm{VaR}_{\beta}\right]\\&=\mathrm{VaR}_{\beta}+\frac{1}{1-\beta}\sum_{n=1}^{N}P_n\left[f(X,\xi)-\mathrm{VaR}_{\beta},0\right]^{+}\end{aligned} \tag{52}$$

$$\left[f(X,\xi)-\mathrm{VaR}_{\beta},0\right]^{+}=\max\left\{f(X,\xi)-\mathrm{VaR}_{\beta},0\right\} \tag{53}$$

where N is the total number of discrete segments; P_n is the probability of occurrence of the n-th segment.

The above equation to solve CVaR needs to calculate VaR at the same confidence level first, which brings inconvenience to the calculation. According to Ref [33], the following optimization problem is constructed.

$$\min f(X,z)=z+\frac{1}{1-\beta}\sum_{n=1}^{N}P_n[f(X,\xi)-z]^{+} \tag{54}$$

By solving the above problem, the minimum value of the objective function is CVaR, and the corresponding z is VaR.

4.2. Objective function

The day-ahead dispatch of IES should pursue both minimizing the desired total cost and avoiding the possible potential risks as much as possible. To address the random variables in the model, this study uses a stochastic optimization method based on scenario analysis to consider the expected values, and s different scenarios are obtained using scenario generation and scenario reduction methods. Therefore, this study utilizes CVaR for risk aversion, which is co-optimized with the expected total cost through a linear combination.

The transformed objective function is:

$$\min F=\omega\mathbb{E}_{\mathbb{p}}[C_{\mathrm{total}}(s)]+(1-\omega)C_{\mathrm{CVaR}} \tag{55}$$

The objective function consists of two components, expected cost $\mathbb{E}_{\mathbb{p}}[C_{\mathrm{total}}]$ and risk costC_{CVaR}, which are assigned subjective weights $\omega(0\leqslant\omega\leqslant1)$ and$1-\omega$. ω is the risk preference coefficient.

In scenario s, the total costs $C_{\mathrm{toal}}(s)$ mainly include generation costsC^{s}_{ele}, gas purchase costsC^{s}_{gas}, wind abandonment penaltiesC^{s}_{pen}, unit start-up and shutdown costsC^{s}_{uni}, CCS cost C^{s}_{CCS} and carbon trading costsC^{s}_{CET}.

$$C_{\mathrm{toal}}(s)=C^{s}_{\mathrm{ele}}+C^{s}_{\mathrm{gas}}+C^{s}_{\mathrm{pen}}+C^{s}_{\mathrm{uni}}+C^{s}_{\mathrm{CCS}}+C^{s}_{\mathrm{CET}} \tag{56}$$

$$C^{s}_{\mathrm{ele}}=\sum_{t\in\mathcal{T}}\sum_{l\in\Omega^{\mathrm{TP}}}\varepsilon^{\mathrm{TP}}\left[a_l^{\mathrm{TP}}+b_l^{\mathrm{TP}}P_{l,t}^{\mathrm{TP}}+c_l^{\mathrm{TP}}\left(P_{l,t}^{\mathrm{TP}}\right)^2\right] \tag{57}$$

$$C^{s}_{\mathrm{gas}}=\sum_{t\in\mathcal{T}}\sum_{l\in\Omega^{\mathrm{GS}}}\varepsilon^{\mathrm{GS}}V_{l,t}^{\mathrm{GS}} \tag{58}$$

$$C^{s}_{\mathrm{pen}}=\sum_{t\in\mathcal{T}}\sum_{l\in\Omega^{\mathrm{WT}}}\varepsilon^{\mathrm{WT}}_{\mathrm{pen}}\left(P_{l,t}^{\mathrm{WT,shed}}-P_{l,t}^{\mathrm{PtG}}\right) \tag{59}$$

$$C^{s}_{\mathrm{uni}}=\sum_{t\in\mathcal{T}}\sum_{l\in\Omega^{\mathrm{TP}}\cup\Omega^{\mathrm{GT}}}\left(S_{Tl}u_{l,t}^{\mathrm{on}}+S_{Dl}u_{l,t}^{\mathrm{off}}\right) \tag{60}$$

$$C^{s}_{\mathrm{CCS}}=\chi_{\mathrm{ct}}\sum_{t\in\mathcal{T}}V_{\mathrm{CO_2}}^{\mathrm{cs}}(t) \tag{61}$$

where $\varepsilon^{\mathrm{TP}}$ is the coal purchase cost factor; $\varepsilon^{\mathrm{GS}}$ represents the gas purchase factor; $\varepsilon^{\mathrm{WT}}_{\mathrm{pen}}$ is the penalty factor of wind curtailment; S_{Tl} and S_{Dl} is the start-stop cost factor of the unit, $u_{l,t}^{\mathrm{on}}$ and $u_{l,t}^{\mathrm{off}}$ is the start-stop status, mainly including TP and GT; χ_{ct} is the cost factor for carbon sequestration.

According to the strategy described in the previous section, the objective function can be transformed into:

$$\min_{X_t,\forall t\in\mathscr{T}} F=\omega\sum_{s\in\mathscr{S}}p_s\left(C^s_{\text{ele}}+C^s_{\text{gas}}+C^s_{\text{pen}}+C^s_{\text{uni}}+C^s_{\text{CET}}\right)+(1-\omega)\left(\xi+\frac{1}{1-\beta}\sum_{s\in\mathscr{S}}p_s\phi_s\right) \tag{62}$$

where $\mathscr{S}$ denotes the set of scenarios in the IES; s denotes the s-th scenario; p_s denotes the probability of occurrence of the s-th scenario; ξ and ϕ_s are an intermediate parameter with no specific physical meaning.

In addition, the auxiliary parameters ϕ_s need to satisfy the following constraints.

$$s.t\begin{cases}\phi_s\geqslant C^s_{\text{ele}}+C^s_{\text{gas}}+C^s_{\text{pen}}+C^s_{\text{uni}}+C^s_{\text{CET}}-\xi\\ \phi_s\geqslant 0\end{cases} \tag{63}$$

4.3. Linearization of natural gas pipeline flow equations

In this section, the natural gas pipeline is handled by a segmented linearization method, thus transforming the natural gas model into a mixed integer linear programming model. Eq. (10) is a nonlinear constraint, specified as:

$$V_{ij,t}=K_{ij}S_{ij,t}\sqrt{S_{ij,t}\left(p^2_{i,t}-p^2_{j,t}\right)},\forall(i,j)\in\mathscr{N}_g,\forall ij\in\mathscr{L}_g \tag{64}$$

By squaring the left and right sides and replacing the sign function, we get:

$$V_{ij,t}\left|V_{ij,t}\right|=K^2_{ij}\left(p^2_{i,t}-p^2_{j,t}\right),\forall(i,j)\in\mathscr{L}_g \tag{65}$$

Let $\varepsilon_{i,t}=p^2_{i,t}$, the air pressure constraint Eq. (13) is:

$$\underline{p}^2_i\leqslant\varepsilon_{i,t}\leqslant\overline{p}^2_i,\forall i\in\mathscr{N}_g \tag{66}$$

At the same time, for the nonlinear problem of pipe flow, let $f(V_{ij,t})=V_{ij,t}\left|V_{ij,t}\right|$, then:

$$f\left(V^{\text{grid}}_{ij,t}\right)=K^2_{ij}\left(\varepsilon_{i,t}-\varepsilon_{j,t}\right),\forall(i,j)\in\mathscr{L}_g \tag{67}$$

Fig. 7 shows the piecewise linearization of quadratic function. Using the incremental segmented linearization to deal with $f(V_{ij,t})$, first select the appropriate number of segmented intervals N_L-1, we can get the discrete points $V^1_{ij,t}, V^2_{ij,t},\ldots,V^{N_L}_{ij,t}$ in the range of values respectively. Next, define the interval auxiliary variables as $d_k\in[0,1]$, μ_k is binary variable, and linearize each interval by segmenting.

$$V_{ij,t}=V^1_{ij,t}+\sum_{k=1}^{N_L-1}\left(V^{k+1}_{ij,t}-V^k_{ij,t}\right)d_k,\forall(i,j)\in\mathscr{L}_g \tag{68}$$

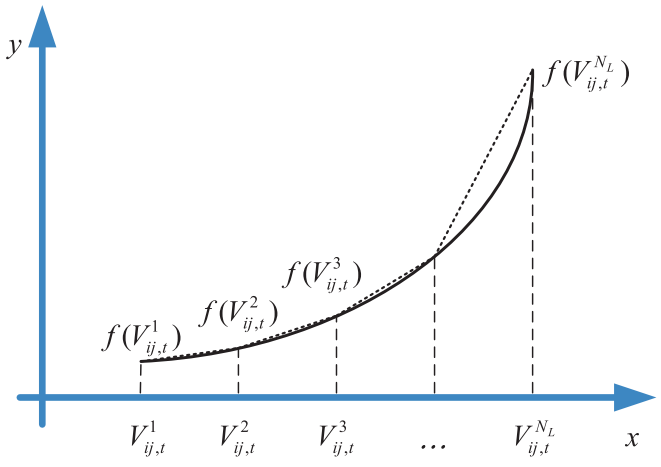

Fig. 7. Piecewise linearization of quadratic function.

$$f\left(V_{ij,t}\right)=f\left(V^1_{ij,t}\right)+\sum_{k=1}^{N_L-1}\left[f\left(V^{k+1}_{ij,t}\right)-f\left(V^k_{ij,t}\right)\right]d_k \tag{69}$$

$$0\leqslant d_k\leqslant 1 \tag{70}$$

$$d_{k+1}\leqslant\mu_k\leqslant d_k \tag{71}$$

Eq. (68) and Eq. (69) describe the optimization variables using the values of the coordinates of the nodes at the ends of each segment and the segment position variables. Eq. (70) represents each segment position variable constraint; Eq. (71) is used to ensure that each segment interval is filled in order from left to right. Similarly, the multinomial function in the objective function can be converted into a linear function by segmental linearization out of force.

4.4. Low carbon economy dispatch model

To cope with the uncertainty of wind power output and multi-energy load, this study proposes a low-carbon economic dispatch model based on CVaR. The model consists of two components, expectation cost and risk cost, in compact form as follows:

$$\begin{aligned}\min_{X_t,\forall t\in\mathscr{T}} F&=\omega\sum_{s\in\mathscr{S}}p_s\mathbf{a}^{\mathrm{T}}\mathbf{x}_s+(1-\omega)(\xi+\frac{1}{1-\beta}\sum_{s\in\mathscr{S}}p_s\phi_s)\\ s.t.\quad&\mathbf{D}\mathbf{x}_s\leqslant\mathbf{d},\forall s\in\mathscr{S}\\ &\mathbf{F}\mathbf{x}_s=\mathbf{g},\forall s\in\mathscr{S}\\ &\phi_s\geqslant\mathbf{a}^{\mathrm{T}}\mathbf{x}_s-\xi,\forall s\in\mathscr{S}\\ &\phi_s\geqslant 0,\forall s\in\mathscr{S}\end{aligned} \tag{72}$$

where $\boldsymbol{x}_s$ denotes the decision variable, which the daily operating outputs of various types of coupling devices under different scenarios; $\boldsymbol{a}$ is the constant coefficient matrix corresponding to the objective function, which is specifically the respective cost coefficients in the objective function; $\boldsymbol{D}$ and $\boldsymbol{F}$ are the coefficient matrices of the variables; $\boldsymbol{d}$ and $\boldsymbol{g}$ are the constant column vectors.

In the constraints, the first constraint denotes the inequality constraint related to the decision variables, mainly including the energy balance constraint and the input–output constraint of the coupling element; the second constraint denotes the equation constraint, mainly including the upper and lower bound constraints of the coupling element; the last two constraints are the conditions to be satisfied by the intermediate parameters.

Fig. 8 shows the computational procedure of the scheduling model. First, the error scenarios are generated based on the Monte Carlo method of Latin hypercube sampling, and the scenarios are reduced by k-medoid clustering. Second, the IES with PtG-CCS is established and converted into a MILP model by segmental linearization. Finally, the CVaR method is used to calculate the risk cost and obtain the optimal scheduling solution.

5. Case study

YALMIP and CPLEX is used to build the mathematical model and Cplex solver is called to solve it. The hardware environment of the test system is AMD Ryzen 7 5800H (3.2 GHz) with 16G of memory.

5.1. System configuration

Fig. 9 shows the 39-20-6 IES diagram. The example is an integrated energy system consisting of a modified 39-node grid[34], a 20-node gas network[35], and a 6-node thermal network [36] coupled together. The power supply units in the power system are CHP at node 30, GT at nodes 33 and 37, which obtain natural gas from nodes 6, 9 and 10 of the natural gas system, respectively, while the other fuel units are TP units.

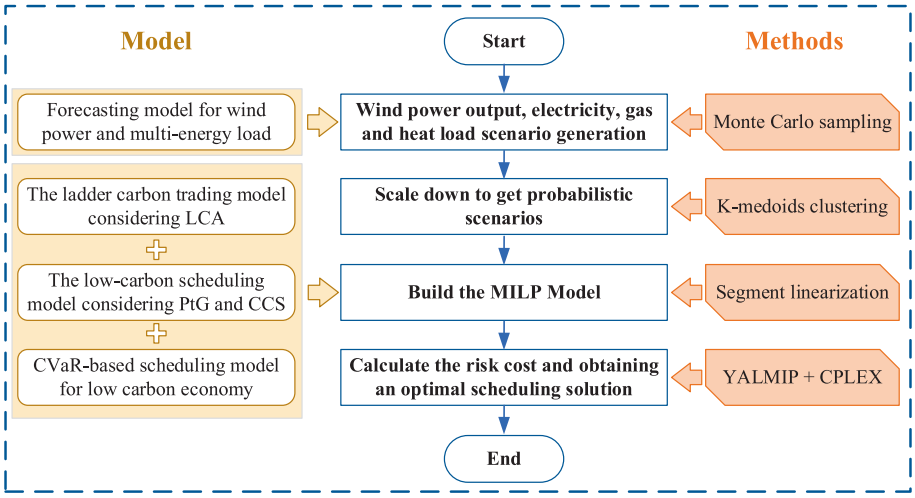

Fig. 8. Calculation Flowchart of Scheduling Model.

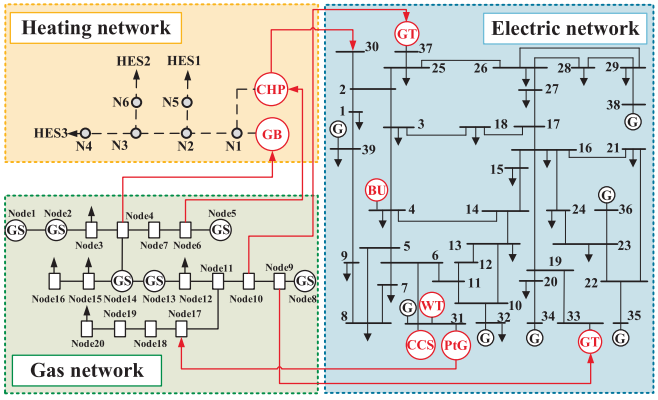

Fig. 9. 39-20-6 Integrated Energy System Diagram.

Both CHP and GB are connected as heat sources at node 1 of the heat network for heat supply. The TP at node 31 was converted to CSS and connected to the gas system through PtG.

Tables 1 and 2 show the specific system simulation parameters and carbon correlation coefficients. Table 3 shows the sources of carbon emission parameters for the LCA energy chain, with reference to the relevant parameters for different energy sources at each stage, respectively.

Fig. 10 shows the forecast data of wind power and load. In dealing with the uncertainty of wind power output and load fluctuations, the deviations are assumed to follow a normal distribution with a mean value of 0. Since wind power output fluctuations are generally larger than load fluctuations, the wind power variance is set to 5 % of the predicted value and the load variance is set to 3 %. A total of 10,000 error scenes are generated based on Monte Carlo method, and 50 typical scenes are obtained by k-medoid clustering.

Table 1
System Simulation Parameters.

GT	$\eta_e^{GT} = 0.35$	$\eta_h^{GT} = 0.50$
CHP	$\eta_e^{CHP} = 0.35$	$\eta_h^{CHP} = 0.50$
PtG	$\overline{P}_e^{PtG} = 1$ MW	$\eta^{PtG} = 0.70$ [37]
	$\phi_{H_2,CO_2}^{PtG} = 0.25$ [38]	$\phi_{H_2,CH_4}^{PtG} = 0.25$ [38]
BU	$\eta_{in}^{BU} = 0.90$	$\eta_{out}^{BU} = 0.90$
	$\overline{P}_{e,in}^{BU} = \overline{P}_{e,out}^{BU} = 120$ kW	$C_e^{BU} = 500$ kWh
	$\underline{S}_e^{BU} = 0.1$	$\overline{S}_e^{BU} = 0.9$
CCS	$\overline{V}_{CO_2}^{CCS} = 1$ Mm^3	$C_e^{BU} = 4$ Mm^3
	$\underline{S}_{CO_2}^{CCS} = 0.05$	$\overline{S}_{CO_2}^{CCS} = 0.95$
Cost factor	$\epsilon_{pen}^{WT} = 50$ \$/MWh	$\epsilon^{GS} = 8.5$ \$/m^3
	$\omega = 0.5$	$\chi_{ct} = 20$ \$/t [39]
Calorific value coefficient	$\epsilon_{gas}^{LHV} = 9.78$ kWh/m^3	$\epsilon_{H_2}^{LHV} = 2.994$ kWh/m^3

Table 2
Carbon related parameters.

TP	$\chi_e^{TP} = 0.798$ t/MWh	$a_1 = 0.00034$, $b_1 = 0.9$, $c_1 = 5$
GT	$\chi_e^{GT} = 0.305$ t/MWh	$a_2 = 0.00025$, $b_2 = -0.004$, $c_2 = 3$
CHP	$\chi_e^{CHP} = \chi_h^{CHP} = 0.305$ t/MWh	$a_3 = 0.00025$, $b_3 = -0.004$, $c_3 = 3$
GB	$\chi_h^{GB} = 0.065$ t/MWh	$\chi_a^{GB} = 0.102$ t/MWh
CET	$\lambda = 20$\$/t [39]	$\alpha = 0.25$

Table 3
LCA Carbon Emission Parameters.

Energy	Type	Reference	Parameters (g/kWh)
Coal	production	[40,41]	$\sigma_{pe} = 112.30$
Coal	transportation	[42–44]	$\sigma_{te} = 6.94$
Natural gas	production	[32,40]	$\sigma_{pg} = 90.19$
Natural gas	transportation	[44–46]	$\sigma_{tg} = 28.80$
Wind	production	[46]	$\sigma_{pw} = 39.72$
Wind	transportation	[46]	$\sigma_{tw} = 3.28$

5.2. Analysis of ladder-type CET mechanism

5.2.1. Benefit analysis of ladder-type CET mechanism

In order to verify the validity of the ladder-type CET model, the PtG-CCS coupling was not considered in the model, and three cases were set up for comparative analysis.

Case 1. *Under the traditional CET, the carbon trading cost is not considered in the objective function.*

Case 2. *Under the traditional CET, the carbon trading cost is considered in the objective function.*

Case 3. *Under the ladder-type CET, the carbon trading cost is considered in the objective function.*

Table 4. shows the optimized scheduling costs for case 1, 2, and 3,

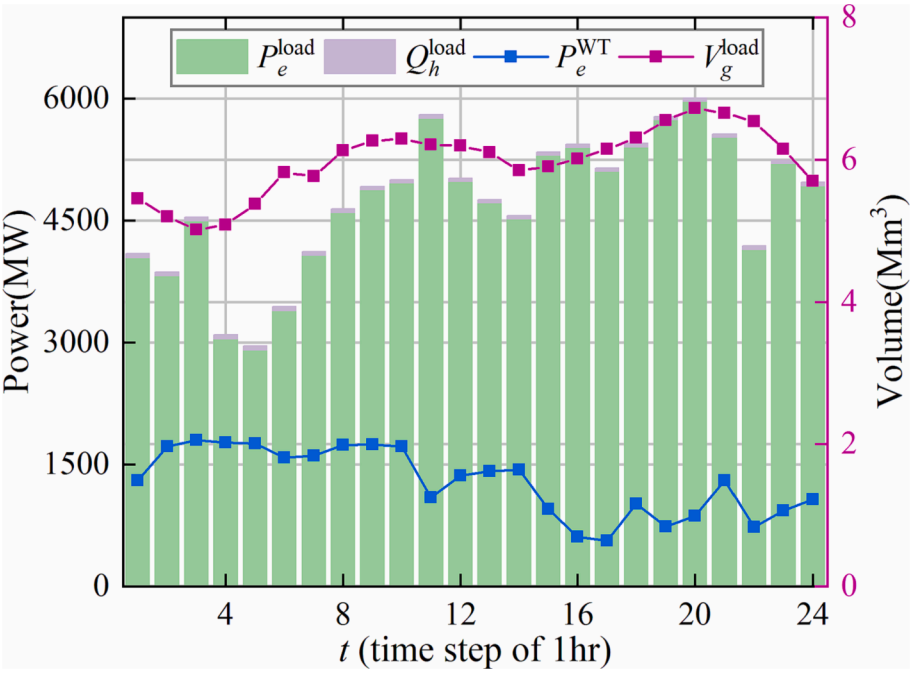

Fig. 10. Forecast values of wind power and load.

Table 4
scheduling cost under different CET mechanisms.

Case	Totalcost(×10^4$)	Start-up cost (×10^4$)	TPcost(×10^4$)	Gascost (×10^4$)	Carbon cost (×10^4$)	WTcost (×10^4$)
1	**1293.24**	0.20	181.17	1071.28	39.05	1.55
2	**1292.77**	0.21	180.52	1072.22	38.26	1.56
3	**1306.62**	0.22	181.39	1072.51	50.93	1.56

and Table 5 shows the carbon emissions and carbon quotas for the three cases. For comparison, Case 1 is calculated with carbon trading costs in the statistics. Combining the two tables, both Case 2 and Case 3 have less carbon emissions than Case 1, which indicates that including carbon emissions into the trading market can effectively reduce carbon emissions. Compared with Case 2, Case 3 reduces the TP's carbon quota and increases the GT's carbon quota, resulting in lower overall carbon emissions, which is consistent with the reality. In practice, GT is a low carbon unit with lower emissions. The results show ladder-type CET can reduce the overall emissions by directing the output of low-carbon units in the system.

In terms of dispatch costs, the main difference between the 3 cases is reflected in the carbon trading costs. Case 3 has the highest total cost, mainly derived from carbon trading costs, which indicates ladder-type CET causes some economic loss. On the other hand, ladder-type CET has a stronger leading role in carbon reduction, it is more suitable for the common interests of global countries.

5.2.2. *Carbon trading base price sensitivity analysis*

Fig. 11 gives the system costs and carbon emissions at different carbon base prices. As the price increases, the total cost of the system increases and the carbon emissions decrease. This is because the increase in carbon price raises the share of CET cost in the total cost, and the total cost inevitably increases with the same total load. In order to reduce the amount of carbon, IES adjusts more low-carbon units to output as much as possible, making the total emissions slowly decrease. Compared with traditional CET, the total cost of ladder-type CET at the same carbon

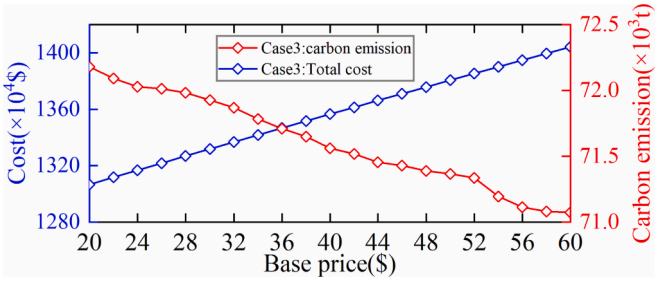

Fig. 11. Total cost and carbon emissions under different base prices.

Table 5
Carbon emission and carbon quota under different CET mechanisms.

Case	Actual Emissions (t)	TP Emissions (t)	GTEmissions (t)	Total quota(t)	TPquota(t)	GTquota(t)
1	**73159.76**	64419.88	8171.29	53636.84	42323.17	10959.12
2	**72614.83**	63827.13	8228.74	53483.05	42023.98	11104.49
3	**72179.58**	63344.36	8276.25	53434.61	41930.07	11149.97

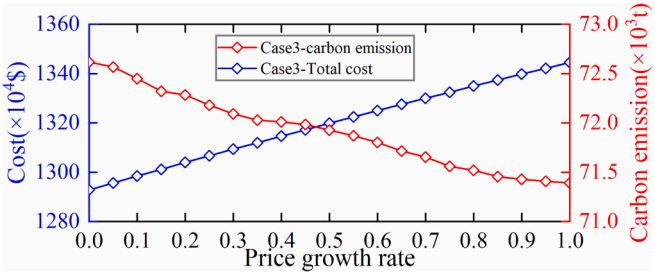

Fig. 12. Total cost and carbon emissions under different price growth rate.

price is higher and emissions is lower.

5.2.3. Transaction price growth rate sensitivity analysis

Fig. 12 presents the effects of different price growth rates on total costs and carbon emissions. As the price growth rate increases, the carbon trading price increases beyond the length of the step interval, and the weight of the emission cost increases. In order to reduce the cost of carbon trading, IES adjusts the output distribution of each equipment to reduce carbon emissions. The increase of both base price and price growth rate can effectively reduce emissions, but it will lose certain economic benefits. Therefore, a reasonable carbon trading base price and price growth rate can effectively guide IES to make carbon emissions.

5.3. PtG-CCS coupling model

5.3.1. Comparison of low carbon performance

In order to verify the economic and low-carbon characteristics of PtG-CCS, the following three cases are added for comparison under the condition of using ladder-type CET.

Case 4. *Only PtG, TP's CO2 is directly discharged into the atmosphere. The CO2 methanated in PtG needs to be purchased at 100$/t.*

Case 5. *Only with CCS, and all CO_2 collected by CCS is sequestered.*

Case 6. *Both P2G and CCS are considered.*

Table 6 and Table 7 show the optimized scheduling costs and carbon emissions for Case 4, 5, and 6, respectively.

The PtG introduced in Case 4 consumes more wind power and reduces the wind curtailment, which in turn reduces the abandonment penalty cost. However, the carbon emissions of Case 4 are higher than Case 3, because the reduced penalty cost is more than the increased carbon transaction cost, so the total system cost is still reduced. Case 5 adds a CCS unit to a single TP, which significantly reduces carbon emissions. Although carbon sequestration by CCS requires a certain cost, it still improves in terms of economics. The economic performance of Case 6 is better than Case 5 because the CO2 collected by CCS can be directly supplied to PtG, eliminating the additional carbon purchase cost, while the introduction of PtG reduces the abandoned wind penalty cost. Case 6 couples PtG and CCS, which achieves the optimum in both economy and environmental friendliness. Therefore, the combination of PtG and CCS can realize the comprehensive use of carbon, which is the most economical and environmentally friendly solution.

5.3.2. Analysis of the effectiveness of the scheduling scheme

Fig. 13 shows the day-ahead dispatching scheme for Case 6. In order to verify the effectiveness of the PtG-CCS optimization scheme, the day-ahead dispatching schemes for the electric, gas and heat networks are obtained.

In Fig. 13(a), TP, GT and WT are used as power sources to undertake the main output of the grid, BU is used for peak shaving and valley filling, and the load side mainly includes grid load, CCS and PtG. The wind power output has an anti-peak effect, with a higher output between 3:00 a.m. and 5:00 a.m., when the electrical load demand is lower and the excess wind power output is absorbed by the PtG. During the period, PtG converts the excess abandoned wind into electricity. Part of the CO2 collected by CCS is directly supplied to PtG for natural gas conversion, and the other part is stored underground. Fig. 13(b) shows the gas network output scheduling scheme, where the gas generated by PtG is matched with the gas source to supply a variety of gas loads. Since the size of heat network is much smaller than gas network, while CHP adopts a "determining power by heat" model for supply, so the gas load has a smaller share of GB and CHP. In the heat network of Fig. 13(c), the heat load is supplied by GB and CHP to achieve heat network balance. In summary, multiple coupling networks can achieve source-load balancing, and the coupling of PtG-CCS effectively promotes the recycling of CO2 and enhances the environmental performance of the IES.

5.4. Cost of risk analysis

5.4.1. The influence of uncertainty factors

There are various uncertainties in IES, and in order to analyze the impact of uncertainty factors, the following cases are set up for comparison when considering both the ladder-type CET and PtG-CCS. In addition, the risk factor is set to 0.5 to equally consider the expected cost and the risk cost.

Case 7. *Consider only wind power uncertainty.*

Case 8. *Consider both wind and load uncertainty.*

Table 8 shows the optimization results for Case 7 and 8. The comprehensive cost of Case 8 is higher than Case 7, where the expected cost increases by $12,900 and the risk cost increases by $122,600, indicating that the economic performance decreases as the uncertainty increases. Therefore, the more uncertainties considered in the model, the more severe the generated scenarios will be, and both the expected cost and risk cost of the system will increase.

5.4.2. The influence of confidence level

Fig. 14 shows the comparison results of CVaR and VaR at different confidence levels. To study the influence of the confidence level on the simulation results, β is made to take values in the interval of [0.9,0.98].

As the confidence level increases, the value of both CVaR and VaR increases systematically, indicating the scheduling risk faced increases. CVaR takes into account the cost of risk that exceeds VaR, so CVaR at the same confidence level is higher than VaR. Meanwhile, the larger the β value is, the larger the rise in CVaR is, because the higher confidence level will lead to a larger risk for IES to take, and the extra risk cost will increase the overall economic cost. The scheduling strategy of IES tends to be conservative and chooses to increase the cost of energy purchase to reduce the risk of uncertainty, resulting in smaller wind power output and larger unit output, so its total operating cost tends to increase

Table 6
Optimized scheduling costs under different operating conditions.

Case	Total cost (×10⁴$)	Start-up cost (×10⁴$)	TPcost (×10⁴$)	Gascost (×10⁴$)	Carbon cost (×10⁴$)	WTcost (×10⁴$)	CCScost (×10⁴$)	CO_2 purchase (×10⁴$)
4	**1305.55**	0.22	181.18	1072.38	50.96	0.53	0.00	0.27
5	**1301.72**	0.22	184.13	1072.51	41.28	2.21	1.38	0
6	**1300.31**	0.22	184.13	1072.38	41.28	0.94	1.36	0

Table 7
Carbon emissions and carbon quotas under different operating conditions.

Case	Actual Emissions (t)	TP Emissions (t)	GTEmissions (t)	CCSEmissions (t)	Total quota(t)	TPquota(t)	GTquota(t)
4	**72230.97**	63396.02	8275.98	0.00	53474.53	41969.97	11149.99
5	**70557.71**	64475.05	8275.98	−2752.29	54147.29	42642.73	11149.99
6	**70557.71**	64475.05	8275.98	−2752.29	54147.29	42642.73	11149.99

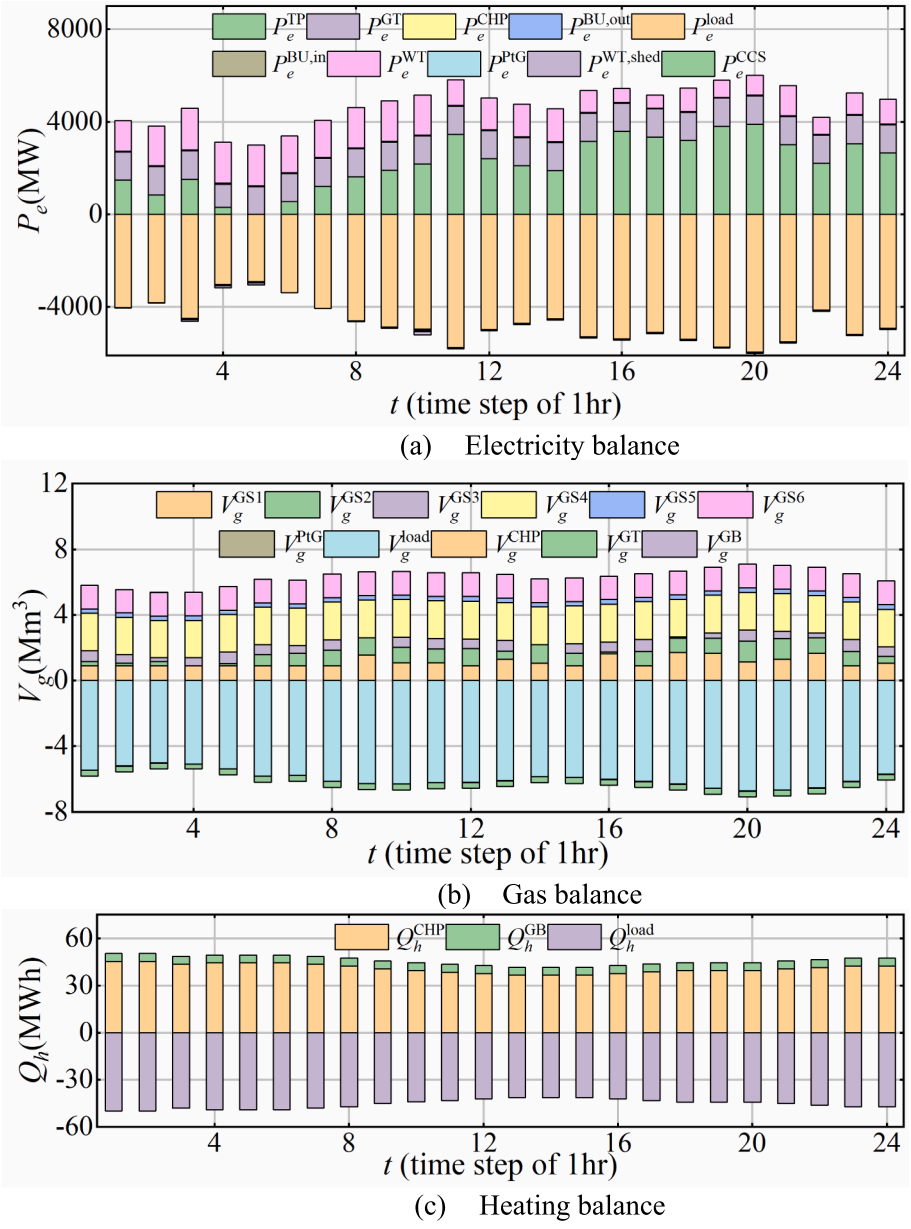

Fig. 13. Day-ahead scheduling strategy for PtG-CCS.

Table 8
Optimization results under different uncertain scenarios.

Case	Comprehensive Cost (×10^4\$)	ExpectedCost (×10^4\$)	CVaR(×10^4\$)	VaR(×10^4\$)	Carbon Emissions (t)
7	**1301.49**	1300.53	1302.44	1301.68	70523.29
8	**1308.27**	1301.84	1314.70	1312.95	70553.76

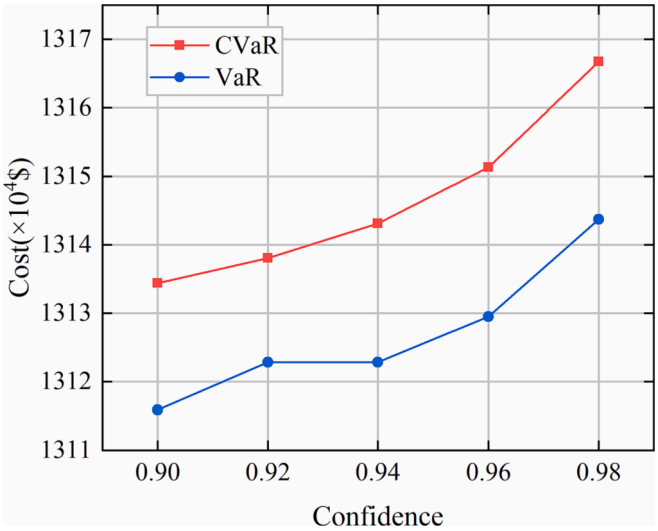

Fig. 14. Comparison of CVaR and VaR among different confidence levels.

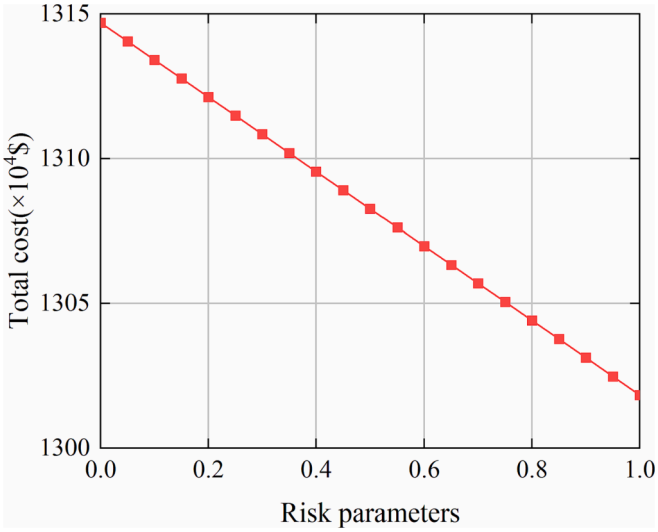

Fig. 15. Relationship between cost and risk preference coefficient.

overall.

5.4.3. *The influence of risk factor*

Fig. 15 reflects the effect of the risk appetite factor on the total cost. As the risk coefficient increases, the integrated system cost gradually decreases, which reflects the importance that decision makers attach to risk. The larger the risk factor is, the less decision makers pay attention to the impact of risk on the system and tend to adopt more risky coexistence scheduling strategies. On the other hand, the increase of system risk will lead to the decrease of system security, so decision makers need to choose the risk appetite factor of the system according to the actual situation.

6. Conclusion

In this study, a low-carbon economic dispatch method considering LCA carbon emissions and risk costs is proposed. To address the issues of incomplete carbon emission measurement and risk loss in IES, LCA and CVaR are introduced in this study. The proposed approach has the following advantages:

(1) The ladder-type CET mechanism can better guide enterprises to reduce carbon emissions and enhance environmental benefits at the expense of certain economic benefits.
(2) The coupling of PtG and CCS can both improve the consumption of new energy and enhance the recycling of CO2, which has a good promotion effect on the economy and environmental protection of IES.
(3) CVaR theory can measure the risk cost of source load uncertainty factors, and the established risk cost function effectively avoids the situation that the economic optimization results are too idealized.
(4) LCA takes into account the carbon emission trajectories of different energy chains and can calculate the actual carbon emissions of IES more comprehensively.

The final result validate the effectiveness and low carbon nature of the proposed method. Therefore, the proposed method is more economical and environmentally friendly than the existing methods, which is a guideline for the development of IES. In addition, considering the integrated demand response in the low-carbon economic dispatch model will be our next work.

CRediT authorship contribution statement

Min Wu: Conceptualization, Data curation, Writing – original draft. **Jiazhu Xu:** Writing – review & editing. **Yun Li:** Resources, Methodology. **Linjun Zeng:** Supervision, Validation. **Zhenglu Shi:** Formal analysis, Writing – review & editing. **Yuxing Liu:** Software, Validation. **Ming Wen:** Project administration, Resources. **Chang Li:** .

Declaration of Competing Interest

The authors declare that they have no known competing financial interests or personal relationships that could have appeared to influence the work reported in this paper.

Data availability

No data was used for the research described in the article.

Acknowledgment

This work was supported by National Natural Science Foundation of China (52077069), and Science-Technology Innovation Platform and Talents Program of Hunan Province, China (2019TP1053).

References

[1] Li J, Li D, Zheng Y, Yao Y, Tang Y. Unified modeling of regionally integrated energy system and application to optimization. Int J Electr Power Energy Syst 2022;134:107377. https://doi.org/10.1016/j.ijepes.2021.107377.
[2] Wu X, Liao B, Su Y, Li S. Multi-objective and multi-algorithm operation optimization of integrated energy system considering ground source energy and solar energy. Int J Electr Power Energy Syst 2023;144:108529. https://doi.org/10.1016/j.ijepes.2022.108529.
[3] Ma H, Chen Q, Hu B, Sun Q, Li T, Wang S. A compact model to coordinate flexibility and efficiency for decomposed scheduling of integrated energy system. Appl Energy 2021;285:116474. https://doi.org/10.1016/j.apenergy.2021.116474.
[4] Liu W, Huang Y, Li Z, Yang Y, Yi F. Optimal allocation for coupling device in an integrated energy system considering complex uncertainties of demand response. Energy 2020;198:117279. https://doi.org/10.1016/j.energy.2020.117279.
[5] Chicco G, Mancarella P. Assessment of the greenhouse gas emissions from cogeneration and trigeneration systems. Part I: Models and indicators. Energy 2008;33:410–7. https://doi.org/10.1016/j.energy.2007.10.006.
[6] Mancarella P, Chicco G. Assessment of the greenhouse gas emissions from cogeneration and trigeneration systems. Part II: Analysis techniques and application cases. Energy 2008;33:418–30. https://doi.org/10.1016/j.energy.2007.10.008.
[7] Dong W, Lu Z, He L, Geng L, Guo X, Zhang J. Low-carbon optimal planning of an integrated energy station considering combined power-to-gas and gas-fired units

equipped with carbon capture systems. Int J Electr Power Energy Syst 2022;138:107966. https://doi.org/10.1016/j.ijepes.2022.107966.
[8] Cheng X, Zheng Y, Lin Y, Chen L, Wang Y, Qiu J. Hierarchical operation planning based on carbon-constrained locational marginal price for integrated energy system. Int J Electr Power Energy Syst 2021;128:106714. https://doi.org/10.1016/j.ijepes.2020.106714.
[9] Yang G, Jiang Y, You S. Planning and operation of a hydrogen supply chain network based on the off-grid wind-hydrogen coupling system. Int J Hydrog Energy 2020;45:20721–39. https://doi.org/10.1016/j.ijhydene.2020.05.207.
[10] Alizad E, Rastegar H, Hasanzad F. Dynamic planning of Power-to-Gas integrated energy hub considering demand response programs and future market conditions. Int J Electr Power Energy Syst 2022;143:108503. https://doi.org/10.1016/j.ijepes.2022.108503.
[11] Bailera M, Lisbona P, Llera E, Peña B, Romeo LM. Renewable energy sources and power-to-gas aided cogeneration for non-residential buildings. Energy 2019;181:226–38. https://doi.org/10.1016/j.energy.2019.05.144.
[12] Chen Z, Zhang Y, Ji T, Cai Z, Li L, Xu Z. Coordinated optimal dispatch and market equilibrium of integrated electric power and natural gas networks with P2G embedded. J Mod Power Syst Clean Energy 2018;6:495–508. https://doi.org/10.1007/s40565-017-0359-z.
[13] Zhang R, Yan K, Li G, Jiang T, Li X, Chen H. Privacy-preserving decentralized power system economic dispatch considering carbon capture power plants and carbon emission trading scheme via over-relaxed ADMM. Int J Electr Power Energy Syst 2020;121:106094. https://doi.org/10.1016/j.ijepes.2020.106094.
[14] Costamagna P. Three-pipeline gas grid: A new concept for power-to-gas associated with complete carbon capture and utilization. Energy Convers Manag 2021;229:113739. https://doi.org/10.1016/j.enconman.2020.113739.
[15] Zhu X, Yang J, Zhan X, Sun Y, Zhang Y. Cloud-edge collaborative distributed optimal dispatching strategy for an electric-gas integrated energy system considering carbon emission reductions. Int J Electr Power Energy Syst 2022;143:108458. https://doi.org/10.1016/j.ijepes.2022.108458.
[16] Xiang Y, Wu G, Shen X, Ma Y, Gou J, Xu W, et al. Low-carbon economic dispatch of electricity-gas systems. Energy 2021;226:120267. https://doi.org/10.1016/j.energy.2021.120267.
[17] Abdallah T, Farhat A, Diabat A, Kennedy S. Green supply chains with carbon trading and environmental sourcing: Formulation and life cycle assessment. Appl Math Model 2012;36:4271–85. https://doi.org/10.1016/j.apm.2011.11.056.
[18] Research on carbon emission reduction benefit of wind power project based on life cycle assessment theory. Renew Energy 2020;155:456–68. https://doi.org/10.1016/j.renene.2020.03.133.
[19] Zeng L, Xu J, Wu M, Tang J, Wu Q, Wang Q, et al. Day-ahead interval optimization for CCHP system considering uncertainty of wind power and PV. Int J Electr Power Energy Syst 2022;138:107895. https://doi.org/10.1016/j.ijepes.2021.107895.
[20] Wang S, Yuan S. Interval optimization for integrated electrical and natural-gas systems with power to gas considering uncertainties. Int J Electr Power Energy Syst 2020;119:105906. https://doi.org/10.1016/j.ijepes.2020.105906.
[21] Haddadian H, Noroozian R. Multi-microgrids approach for design and operation of future distribution networks based on novel technical indices. Appl Energy 2017;185:650–63. https://doi.org/10.1016/j.apenergy.2016.10.120.
[22] Zhu F, Zhong P, Xu B, Liu W, Wang W, Sun Y, et al. Short-term stochastic optimization of a hydro-wind-photovoltaic hybrid system under multiple uncertainties. Energy Convers Manag 2020;214:112902. https://doi.org/10.1016/j.enconman.2020.112902.
[23] Thang VV, Ha T, Li Q, Zhang Y. Stochastic optimization in multi-energy hub system operation considering solar energy resource and demand response. Int J Electr Power Energy Syst 2022;141:108132. https://doi.org/10.1016/j.ijepes.2022.108132.
[24] Zhang Y, Campana PE, Lundblad A, Zheng W, Yan J. Planning and operation of an integrated energy system in a Swedish building. Energy Convers Manag 2019;199:111920. https://doi.org/10.1016/j.enconman.2019.111920.
[25] Chen L, Tang H, Wu J, Li C, Wang Y. A robust optimization framework for energy management of CCHP users with integrated demand response in electricity market. Int J Electr Power Energy Syst 2022;141:108181. https://doi.org/10.1016/j.ijepes.2022.108181.
[26] Rezaei N, Kalantar M. Stochastic frequency-security constrained energy and reserve management of an inverter interfaced islanded microgrid considering demand response programs. Int J Electr Power Energy Syst 2015;69:273–86. https://doi.org/10.1016/j.ijepes.2015.01.023.
[27] Wu J, Zhang B, Deng W, Zhang K. Application of Cost-CVaR model in determining optimal spinning reserve for wind power penetrated system. Int J Electr Power Energy Syst 2015;66:110–5. https://doi.org/10.1016/j.ijepes.2014.10.051.
[28] Tan Z, Wang G, Ju L, Tan Q, Yang W. Application of CVaR risk aversion approach in the dynamical scheduling optimization model for virtual power plant connected with wind-photovoltaic-energy storage system with uncertainties and demand response. Energy 2017;124:198–213. https://doi.org/10.1016/j.energy.2017.02.063.
[29] MansourLakouraj M, Shahabi M, Shafie-khah M, Ghoreishi N, Catalão JPS. Optimal power management of dependent microgrid considering distribution market and unused power capacity. Energy 2020;200:117551. https://doi.org/10.1016/j.energy.2020.117551.
[30] Alabdulwahab A, Abusorrah A, Zhang X, Shahidehpour M. Coordination of Interdependent Natural Gas and Electricity Infrastructures for Firming the Variability of Wind Energy in Stochastic Day-Ahead Scheduling. IEEE Trans Sustain Energy 2015;6:606–15. https://doi.org/10.1109/TSTE.2015.2399855.
[31] Udo de Haes HA, Heijungs R. Life-cycle assessment for energy analysis and management. Appl Energy 2007;84:817–27. https://doi.org/10.1016/j.apenergy.2007.01.012.
[32] Wang R, Wen X, Wang X, Fu Y, Zhang Y. Low carbon optimal operation of integrated energy system based on carbon capture technology, LCA carbon emissions and ladder-type carbon trading. Appl Energy 2022;311:118664. https://doi.org/10.1016/j.apenergy.2022.118664.
[33] Uryasev S. Conditional value-at-risk: optimization algorithms and applications. Proc. IEEEIAFEINFORMS 2000 Conf. Comput. Intell. Financ. Eng. CIFEr Cat No00TH8520, 2000, p. 49–57. https://doi.org/10.1109/CIFER.2000.844598.
[34] Zimmerman RD, Murillo-Sanchez CE, Thomas RJ. MATPOWER: Steady-State Operations, Planning, and Analysis Tools for Power Systems Research and Education. IEEE Trans Power Syst 2011;26:12–9. https://doi.org/10.1109/TPWRS.2010.2051168.
[35] De Wolf D, Smeers Y. The Gas Transmission Problem Solved by an Extension of the Simplex Algorithm. Manag Sci 2000;46:1454–65. https://doi.org/10.1287/mnsc.46.11.1454.12087.
[36] Li Z, Wu W, Wang J, Zhang B, Zheng T. Transmission-Constrained Unit Commitment Considering Combined Electricity and District Heating Networks. IEEE Trans Sustain Energy 2016;7:480–92. https://doi.org/10.1109/TSTE.2015.2500571.
[37] Ge L, Liu H, Yan J, Zhu X, Zhang S, Li Y. Optimal Integrated Energy System Planning with DG Uncertainty Affine Model and Carbon Emissions Charges. IEEE Trans Sustain Energy 2021:1. https://doi.org/10.1109/TSTE.2021.3139109.
[38] He L, Lu Z, Zhang J, Geng L, Zhao H, Li X. Low-carbon economic dispatch for electricity and natural gas systems considering carbon capture systems and power-to-gas. Appl Energy 2018;224:357–70. https://doi.org/10.1016/j.apenergy.2018.04.119.
[39] Ji Z, Kang C, Chen Q, Xia Q, Jiang C, Chen Z, et al. Low-Carbon Power System Dispatch Incorporating Carbon Capture Power Plants. IEEE Trans Power Syst 2013;28:4615–23. https://doi.org/10.1109/TPWRS.2013.2274176.
[40] Zhou H, Qian Y, Kraslawski A, Yang Q, Yang S. Life-cycle assessment of alternative liquid fuels production in China. Energy 2017;139:507–22. https://doi.org/10.1016/j.energy.2017.07.157.
[41] Zhou H, Yang S, Xiao H, Yang Q, Qian Y, Gao L. Modeling and techno-economic analysis of shale-to-liquid and coal-to-liquid fuels processes. Energy 2016;109:201–10. https://doi.org/10.1016/j.energy.2016.04.108.
[42] Ou X, Xiaoyu Y, Zhang X. Life-cycle energy consumption and greenhouse gas emissions for electricity generation and supply in China. Appl Energy 2011;88:289–97. https://doi.org/10.1016/j.apenergy.2010.05.010.
[43] Li X, Ou X, Zhang X, Zhang Q, Zhang X. Life-cycle fossil energy consumption and greenhouse gas emission intensity of dominant secondary energy pathways of China in 2010. Energy 2013;50:15–23. https://doi.org/10.1016/j.energy.2012.12.020.
[44] Li X, Zhou H, Wang Y, Qian Y, Yang S. Thermoeconomic analysis of oil shale retorting processes with gas or solid heat carrier. Energy 2015;87:605–14. https://doi.org/10.1016/j.energy.2015.05.045.
[45] Xiang D, Yang S, Li X, Qian Y. Life cycle assessment of energy consumption and GHG emissions of olefins production from alternative resources in China. Energy Convers Manag 2015;90:12–20. https://doi.org/10.1016/j.enconman.2014.11.007.
[46] Wang Z, Shi Y, Tang Y, Men X, Cao J, Wang H. Low carbon economy operation and energy efficiency analysis of integrated energy systems considering LCA energy chain and carbon trading mechanism. Proc CSEE 2019;39(6):1614–26. 10.13334/j.0258-8013.pcsee.180754.